Hindawi
International Journal of Photoenergy
Volume 2022, Article ID 8595591, 14 pages
https://doi.org/10.1155/2022/8595591

Research Article

Thermal Performance of a Dimpled Tube Parabolic Trough Solar Collector (PTSC) with SiO_2 Nanofluid

M. Arun,[1] Debabrata Barik,[1] K. P. Sridhar,[2] and Milon Selvam Dennison[3]

[1]*Department of Mechanical Engineering, Karpagam Academy of Higher Education, Coimbatore 641021, India*
[2]*Department of Electronics and Communication Engineering, Karpagam Academy of Higher Education, Coimbatore 641021, India*
[3]*Department of Mechanical Engineering, Kampala International University, Western Campus, Kampala 20000, Uganda*

Correspondence should be addressed to Debabrata Barik; debabrata93@gmail.com
and Milon Selvam Dennison; milon.selvam@kiu.ac.ug

Received 7 April 2022; Revised 24 June 2022; Accepted 11 August 2022; Published 28 August 2022

Academic Editor: Chuan Li

In this research work, dimple texture tubes and silicon dioxide (SiO_2) nanofluid were used to analyze the performance parameters of a solar water heater. For this purpose, SiO_2 was mixed with deionized (DI) water using an ultrasonic dispersion device to prepare the nanofluids (SiO_2/DI-H_2O). The size of the nanoparticle was in the range of 10-15 nm. Different volume concentrations of the nanoparticles in the range of 0.1% to 0.5%, in steps of 0.1%, were chosen to prepare the nanofluids to carry out the experiments. Apart from this, computational fluid dynamics (CFD) tool was used to numerically analyze the parameters affecting the performance of the solar water heater, as well as the fluid flow pattern in the dimple texture tube. During the experiment, the mass flow rate of the base fluid (water) varied in the range of 0.5 kg/min to 3.0 kg/min in steps of 0.5 kg/min. The added advantage of the dimple texture tube design led to an increase in turbulence in the flow pattern, resulting 34.2% increase in the convective heat transfer efficiency compared with the plain tube. Among all experimental modules, SiO_2/DI-H_2O with a mass flow rate of 2.5 kg/min and 0.3% volume concentration gives overall optimized results in absolute energy absorption, gradient temperature, and efficiency of the solar water heater. The efficiency metrics of the experimental results were compared with the simulation results, and it was in the acceptable range with an overall deviation of ±7.42%.

1. Introduction

Based on the global energy consumption rate, 86% of the global energy is produced from fossil fuels which demands a continuous rise in the requirement for fossil fuels. Consequently, CO_x and NO_x emissions from fossil fuels significantly influence global warming [1]. This circumstance demands the development of renewable energy technology to reduce greenhouse gas emissions and air pollution simultaneously. Solar thermal, geothermal, biomass, marine, solar, and hydropower are a few renewable energy sources globally [2]. A solar collector is an efficient device to capture the maximum solar energy from the sun [3]. The performance of solar thermal systems can be further improved by system optimization, heat transfer enhancement, and operation optimization. The efficient operation of solar thermal systems combined with thermal energy storage systems is the most important aspect of a large-scale solar energy utilization. It should be noted that the utilization of solar thermal energy will substantially impact the building environment.

Flat-plate collectors, evacuated tubes, and parabolic collectors are the common types of solar collectors, and each has its advantages and disadvantages based on the heat transfer rate. Based on the application, the heat transfer tubes in flat-plate and evacuated tube solar collectors vary in shape and size. A vacuum is used to keep the absorption plate within a glass tube in an evacuated solar collector to decrease heat loss due to convection. A greater temperature may be maintained in the evacuated tube solar collector than in the flat-plate collector, which has a lower efficiency [1, 4, 5]. When erection costs are taken into account for solar panels, the solar collector's energy efficiency remains less

[6, 7]. Hence, an increase in the efficiency of the different solar collectors is a prime aspect to be focused on.

The solar thermal systems' effectiveness entirely relies on their collectors' performance. Thermal and photovoltaic systems in the solar collectors are utilized to convert sunlight into heat with the help of working fluids like air or water [8, 9]. From an economic point of view, flat-plate collectors are used to heat the working fluids. But the efficiency and performance are poor. Several researchers have conducted considerable research to increase the efficiency and performance of flat-plate collectors without affecting the cost [10]. Most researchers suggested that utilizing nanofluids in place of ordinary fluids in solar collectors can increase the performance of the flat-plate collectors. Bai et al. [11] investigated nanofluids which are the suspensions of water and nanoparticles in the range of 1–100 nm in size. They identified that this kind of working fluid has a higher thermal conductivity than its base fluid. The use of nanofluids in solar thermal systems has significant positive impacts on environmental, economic, and thermal aspects.

Moravej et al. [12] experimentally investigated the impact of substituting water with surfactant-free water using flat-plate solar collectors with rutile TiO_2–water nanofluids as a working fluid. They followed the ASHRAE standard; as per the standard, the flow rate of the heat transfer fluid (HTF), the sun irradiation, and the temperature difference between the intake and outflow were analyzed. They concluded that the thermal efficiency could be improved by using TiO_2–water nanofluids instead of water alone. Mahian et al. [13] investigated the usage of four different nanofluids (Al_2O_3water, TiO_2/water, SiO_2/water, and Cu/water) in a mini-channel-based solar collector. They found that Cu/water nanofluid exhibits the optimum temperature at the exit and the lowest entropy at the source with an increase in thermal efficiency. Parvin et al. [14] conducted a numerical study to examine the direct absorption collector, direct convection heat transfer efficacy, and entropy production using Cu–water nanofluid as the working fluid. They analyzed the effect of the Nusselt number, entropy generation Bejan number, collector efficiency, and solid volume fraction of nanoparticles on the collector's performance. They identified that isotherms and heat functions for varied solid volume fractions and inertia forces significantly affect the collector's performance.

Noghrehabadi et al. [15] investigated the direct absorption of a flat-plate solar collector by a low-temperature SiO_2/water nanofluid. They evaluated the influence of one of the stable nanofluids on the efficiency of a symmetric collector in light of the previous results. In a flat-plate collector, water and a SiO_2/water nanofluid with a mass fraction of 1% are tested as coolants. They concluded that employing SiO_2/water nanofluid as a coolant increases the collector efficiency by improving its optical and thermophysical characteristics. Ghalambaz et al. [16] investigated the viscosity and thermal conductivity fluctuation of Al_2O_3 nanofluid as a working fluid. They reported that with the increase in the concentration of Al_2O_3 nanofluid, the thermal conductivity increased, and the viscosity of the working fluid decreased. Furthermore, they observed a 12.8% improvement in thermal efficiency while the volume concentration of the nanoparticle was 1%. Sujith et al. [17] studied the thermal conductivity of Al_2O_3 and copper oxide (CuO) nanofluids, and they revealed that the increase in the concentration of the nanofluids significantly affects the thermal conductivity. Furthermore, they observed that the thermal conductivity of CuO nanofluid was greater than that of Al_2O_3 nanofluid at the same concentration ratio.

Verma et al. [18] inspected the effect of thermal performance of a flat-plate solar collector, employing nanofluids of Al_2O_3, CuO, SiO_2, TiO_2, and graphene with multiwall carbon nanotube (MWCNT). They reported that thermal efficiency was enhanced by 23.5% with MWCNT nanofluid as the working medium. Yan et al. [19] investigated the thermal conductivity and transmissivity of the nanofluid of SiO_2 and water with a mass fraction of 1%, 3%, and 5%. They also numerically analyzed the solar-collector vacuum tubes filled with water (5 wt. %) and nanofluid of SiO_2 using a computer model. They identified that the heat transfer properties of the SiO_2/water nanofluid were improved. Also, it was absorbed that the temperature and velocity distributions of the nanofluid of SiO_2 had a significant impact on the heat transfer than that of the ordinary fluids. Yousefi et al. [20] experimentally studied the effects of Al_2O_3/water nanofluid as a working fluid in a flat-plate solar collector. Their study employed the nanofluid with 0.2% and 0.4% weight fraction and 15 nm particle size and a controlled mass flow rate of nanofluid in the range of 1 to 3 litres per minute, giving an increase in thermal efficiency of 28.3% in comparison to pure water.

Sundar and Sharma [21] experimentally investigated the effect of Al_2O_3 nanoparticles in deionized water as working fluid in a solar heater inserted with and without a twisted tap. They conclude that the copper tube channels' thermal efficiency was significantly inserted with a twisted tap. Ekiciler [22] numerically investigated the heat transfer phenomenon of Al_2O_3 nanoparticles with a volume fraction of 1% to 5% in a duct with a backwards-facing step. They observed that the Nusselt number and Reynolds numbers were directly proportional to the increase in the volume percentage of the Al_2O_3 nanoparticles. Thansekhar and Anbumeenakshi [23] studied the effect of nanofluids on the improvement of heat transfer rate in a microchannel heat sink. They identified that a higher volume concentration of Al_2O_3 nanoparticles in the nanofluid exhibits an enhanced heat transfer rate compared to SiO_2 nanoparticles.

Kalidoss et al. [24] focused on Therminol 55-TiO_2 nanofluids for solar energy storage. They utilized Fresnel lenses, secondary reflectors, and a glass-type evacuated absorber tube to improve the photothermal conversion efficiency. They suggested that improvement in nanofluid concentration enhances the thermal conductivity, and the significance of optical absorbance indicates nanofluids' stability. Cardoso et al. [25] evaluated the influence of TiO_2/SiO_2 nanoparticles in terms of surface area, SEM/TEM morphology, and phase transaction temperature. They found that photoanodes with 3% SiO_2 are more efficient due to increased surface area, and SiO_2 passivation of imperfections increases the photocurrent. Ayoobi and Ramezanizadeh [26] documented the performance and efficiency of the solar still combined with a flat-plate collector in terms of energy, exergy, economic,

and productivity. They observed that maximum efficiency of 60% was obtained in the flat-plate collector by improving the evaporation rate with the aid of six microcompartments in the collector basin. Cao et al. [27] numerically investigated the entropic properties of flat-plate solar collector (FPSC) with the number of swirls generating nozzles. They predicted the overall system performance using N_E, N_S, Nu, and heat transfer improvement (HTI). They found that the maximum value of HTI and efficiency were 1.7 and 0.9, respectively, for the quad nozzle.

From the extensive literature review on the relevance to the present works, it was observed that many authors had adopted various methods to improve the performance of solar water heaters by using the following techniques such as varying nanoparticles size, use of mini-channel-based solar collector, adoption of multiwall carbon nanotube, use of twisted tap design, and use of microchannel heat sink. It was clear that none of the researchers has used dimple texture tubes with nanoparticles for performance improvement analysis and has not documented computational analysis for dimpled tube texture using CFD.

In the present investigation, the authors have presented a numerical and experimental analysis of a parabolic plate solar water heater using a tube in tube type heat exchanger, with a dimple inner tube having a P/D ratio of 3. Also, the authors have used deionized water and nanoparticles of SiO_2 of size 10-15 nm at volume concentrations of 0.1 to 0.5% in steps of 1% to prepare the nanofluid. During the investigation, the mass flow rate of the water in the tube was varied in the range of 0.5 kg/min to 3.0 kg/min in steps of 0.5 kg/min to analyze the absolute energy of the parabolic collector, heat loss from the dimpled tube, parabolic collector efficiency, gradient temperature of the dimpled tube, friction factor for the working fluid, Reynolds number, Nusselt number, and convective heat transfer coefficient of the dimpled tube. Also, the velocity, temperature, and pressure contour of the PTSC were analyzed using CFD.

2. Material and Methods

In the present investigation, the performance parameters of a parabolic trough solar collector (PTSC) were analyzed using SiO_2 nanoparticles with deionized water. The concentration of the nanoparticles varied in the range of 0.1 to 0.5% in steps of 1%. Apart from this, the copper tube of the solar water heater was modified to make dimples on it to create more turbulence in the working fluid. Also, the mass flow rate of the water in the tube was varied as 0.5 kg/min, 1.0 kg/min, 1.5 kg/min, 2.0 kg/min, 2.5 kg/min, and 3.0 kg/min to analyze the absolute energy of the parabolic collector, heat loss from the dimpled tube, parabolic collector efficiency, gradient temperature of the dimpled tube, friction factor for the working fluid, Reynolds number, Nusselt number, and convective heat transfer coefficient of the dimpled tube. Also, the performance parameters of a PTSC were analyzed by using the CFD tool (Fluent 18.0). The experimental and the numerical results were compared and presented in subsequent sections.

2.1. Design and Experimental Setup. The experimental setup used in this present research is a geometric model consisting of a dimpled tube of 1200 mm in length and 50 mm in diameter, connected to a circular 1500-litre reservoir containing working fluids, as shown in Figure 1. The solar radiation strength of the outer dimpled tube was 847 W/m^2, and it provided a steady heat flow with a turbulent flow of 500 W/m^2. SiO_2/DI-H_2O was used as nanofluid in the present investigation, and it has a volume concentration of 0.1-0.5% in steps of 0.1%. The dimple diameter chosen for making the dimple was 0.05 mm. The dimples were fabricated on the outer surface of the tube with the help of a screw-type punching die made of cast iron.

The specification of the experimental setup is given in Table 1. The temperature measurements of the glazed solar collector were recorded at an inclination angle of 45°. Two mercury-bar thermometers were fitted to measure the working fluid temperature at the inlet and outlet of the PTSC separately. A positive displacement pump was used to maintain the flow across the PTSC, and the flow was regulated with the help of control valves. The mass flow rate of the working fluid flow was measured with a flow meter, and it varied from 0.5 kg/min to 3.0 kg/min depending on the valve regulation and the stages of the experiment. A sun meter was used to measure the solar radiation intensity, and it was found to be 847 W/m^2.

2.2. Nanofluid Preparation. The nanofluid was made of nanopowder of SiO_2 of 99.7% purity, 20 nm average size, and pH 7, and density was 4170 kg/m^3. The nanofluids were made with 0.1 to 0.5 percent volume of nanoparticles in steps of 0.1% each. The ultrasonic dispersion setup for the nanofluid preparation is shown in Figure 2. By using this setup, the dispersion of the nanoparticles takes place in DI water to avert accumulation and assures a pH of 7. The specifications of the nanoparticles are given in Table 2. SiO_2 nanoparticles have been purified in the ambient air with a mesh size of 0.5 μm. The thermophysical features of nanofluids were compared theoretically and experimentally and explained in subsequent sections. The properties of nanofluids are given in Table 3.

2.3. Governing Equation. The problem statement can be expressed in the form of governing equations [9, 18], as shown below:

$$\frac{du}{dx} + \frac{dv}{dy} + \frac{dw}{dz} = 0. \tag{1}$$

The momentum equations in x, y, and z are as follows [9, 18]:

$$\rho_{SiO_2}\left(\frac{\partial u}{\partial t} + u\frac{\partial u}{\partial x} + v\frac{\partial u}{\partial y} + w\frac{\partial w}{\partial z}\right) = -\frac{\partial p}{\partial x} + \mu\left(\frac{\partial^2 u}{\partial x^2} + \frac{\partial^2 u}{\partial y^2} + \frac{\partial^2 u}{\partial z^2}\right) - \rho_{SiO_2}\propto_{SiO_2} g_x(T - T_{ref}), \tag{2}$$

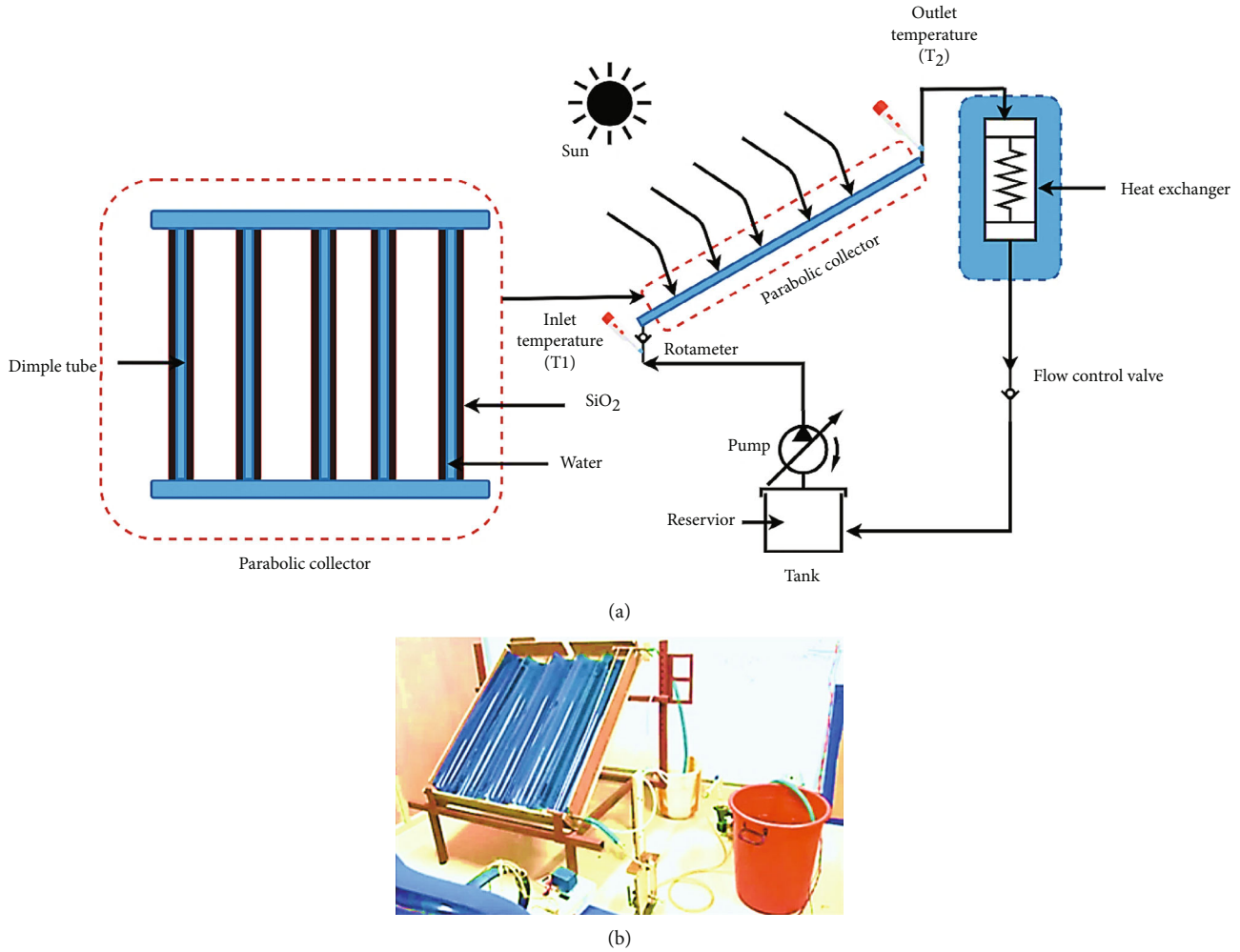

Figure 1: (a) Layout of the experimental setup. (b) Photograph of the experimental setup.

$$\rho_{SiO_2}\left(\frac{\partial v}{\partial t}+u\frac{\partial v}{\partial x}+v\frac{\partial v}{\partial y}+w\frac{\partial v}{\partial z}\right) = -\frac{\partial p}{\partial x}+\mu\left(\frac{\partial^2 v}{\partial x^2}+\frac{\partial^2 v}{\partial y^2}+\frac{\partial^2 v}{\partial z^2}\right)-\rho_{SiO_2}\propto_{SiO_2} g_x(T-T_{ref}), \tag{3}$$

$$\rho_{SiO_2}\left(\frac{\partial w}{\partial t}+u\frac{\partial w}{\partial x}+v\frac{\partial w}{\partial y}+w\frac{\partial w}{\partial z}\right) = -\frac{\partial p}{\partial x}+\mu\left(\frac{\partial^2 w}{\partial x^2}+\frac{\partial^2 w}{\partial y^2}+\frac{\partial^2 w}{\partial z^2}\right)-\rho_{SiO_2}\propto_{SiO_2} g_x(T-T_{ref}). \tag{4}$$

The energy is given by [9, 18]

$$\rho_{SiO_2}\left(\frac{\partial T}{\partial t}+u\frac{\partial T}{\partial x}+v\frac{\partial T}{\partial y}+w\frac{\partial T}{\partial z}\right) = \frac{k_{eff}}{(C_P\cdot\rho)_{SiO_2}}\left(\frac{\partial^2 T}{\partial x^2}+\frac{\partial^2 T}{\partial y^2}+\frac{\partial^2 T}{\partial z^2}\right). \tag{5}$$

The density for both the base fluid and the SiO_2 nanoparticles can be calculated using the correlation presented below [9, 18]:

$$\rho_{SiO_2} = \varphi(C_P\cdot\rho)+(1-\varphi)(\beta\rho)_{SiO_2}. \tag{6}$$

SiO_2 nanofluid's thermal conductivity was calculated using the Maxwell model, which can be expressed in terms of the following equation [9]:

$$\frac{k_{SiO_2}}{k_f} = \frac{2k_f+k_s+2\varphi k_f-2\varphi k_s}{2k_f+k_s-\varphi k_f-\varphi k_s}. \tag{7}$$

The successful dynamic viscosity association of Brinkman has been used in this analysis [9]

$$\mu_{SiO_2} = \frac{\mu_f}{(1-\varphi)^{2.5}}. \tag{8}$$

The evacuated tunnel was cut up and down. Hence, the

Table 1: Specification of the experimental setup.

Specification	Dimensions
Collector length	1800 mm
Width of collector	1200 mm
Length of absorber plate	1650 mm
Thermal conductivity of absorber plate	387 W $(mK)^{-1}$
Width of the absorber plate	1000 mm
Plate thickness	5 cm
The density of plate material	8954 kg/m^3
The diameter of the riser pipe	0.0125 m
The diameter of the header pipe	2.5 cm
The riser and head of thickness	7 cm
Tube centre to centre distance	11.25 cm
Glass and absorber plate between the spacing	30 cm
Thermal conductivity of insulation material	0.044 W $(mK)^{-1}$
The density of the insulation material	200 kg/m^3
The thickness of the insulation material	0.05 m
Area of the absorber plate	960 × 1000 mm
The thickness of the riser tube	1 mm

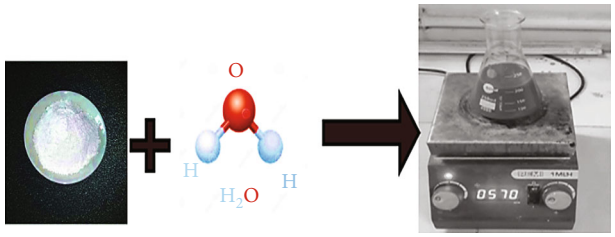

SiO_2 nano power Di-H_2O (De-ionized water) Nanofluid in UP 400S ultrasonic processor

Figure 2: Ultrasonic dispersion setup for the preparation of nanofluid.

heat was applied only to the upper part, where the lower part was unheated. The top portion of the dimpled tube is expected to receive 50% to 57% of solar radiation, while the bottom receives less radiation unless the solar water heater uses the reflector. The solar radiation intensity was recorded from 8 am morning to 5 pm the evening using a sun meter. 952 W/m^2 maximum sunlight radiation intensity had been reached in the afternoon. The heated stream around the dimpled tube has been considered to be 847 W/m^2 in this analysis.

2.4. Grid Independence Test. Fine mesh size and shape are the critical parameters to ensure the accuracy and quick computational time of the CFD numerical calculation. In this analysis, 3D meshes were utilized in the ANSYS platform to analyze the influence of grid numbers on the maximum inside tank temperature. Figure 3 shows the highest temperature within the tank converged at 308 K. In the computational domain, the element size was maintained in the range of 586275.

Table 2: Specification of the nanoparticle.

Properties	Values
Nanoparticle material	SiO_2
Density	4170 kg/m^3
Molar mass of SiO_2	60.0843 g/mol
Nanoparticle size	10-15 nm
Melting point	1986 K
Boiling point	2503 K
Thermal conductivity	1.38 W/mK
Crystal structure	Cristobalite
Purity of nanoparticle	99.7%
Specific surface area	160 m^2/g
Volume density	4170 kg/m^3
Specific heat	880 kJ/kg K

2.5. Performance Analysis. The performance analysis was carried out using two different techniques, and the estimation readings were recorded from 8 am to 5 pm. SiO_2 levels and flow speeds are measured in the dimples tube. The experiments were carried out in six stages to achieve consistency, and each stage consisted of 30 minutes. The collection time constant of 64.25% complies with ASHRAE requirements; each 60-minute cycle was further separated into 20-minute subcycles. Furthermore, the PTSC collector performance was determined by linear regression at a minimum of 20 data points at different inlet water temperatures to carry out the steady-state model. Data was collected regularly for several months.

2.6. Analysis of Collector Efficiency. The collector efficiency reveals the entire radiation of the incident from the opening area, and the collector produces the available heat gain as shown in [9]

$$Q_g = C_{P_{SiO_2}}(T_O - T_I). \tag{9}$$

In Equation (10), the efficiency of solar collector for PTSC has been obtained by [9]

$$\eta_c = \frac{Q_g}{A_a} = \frac{C_{P_{SiO_2}}(T_O - T_I)}{A_a}. \tag{10}$$

The collector performance curve is plotted for a sequence of 16 data points. A linear reverse fitting procedure is used to locate the slope and intercepts. The following equations denote the collector's productivity as shown in [9]

$$\eta_c = \alpha\tau(F_R) - \frac{U_L F_R}{C}\left(\frac{T_O - T_I}{I}\right). \tag{11}$$

As shown in Equation (11), where $F_R(\eta_c) = \alpha\tau(F_R)$ indicates the energy parameter is consumed, $U_L F_R/C$ indicates the parameter of removal energy, and $(T_O - T_I)/I$ indicates the parameter of heat loss or collector's function curve. The relationship between the heat loss parameter and

Table 3: Properties of nanofluids.

Properties	DI H_2O-SiO_2 0.1%	DI H_2O-SiO_2 0.2%	DI H_2O-SiO_2 0.3%	DI H_2O-SiO_2 0.4%	DI H_2O-SiO_2 0.5%
Density, kg/m^3	1014	1025	1029	1035	1042
Specific heat, kJ/kgK	410.6	414.8	418.5	422.7	427.8
Convective heat transfer coefficient, W/m^{2}K	0.6723	0.7562	0.7825	0.8251	0.8452
Viscosity, m^2/s	$0.411e^{-6}$	$0.388e^{-6}$	$0.377e^{-6}$	$0.286e^{-6}$	$0.257e^{-6}$
Boiling point, ˚C	2950	2958	2960	2968	2970
Molar mass, g/mol	60.08	62.72	64.28	66.82	69.86

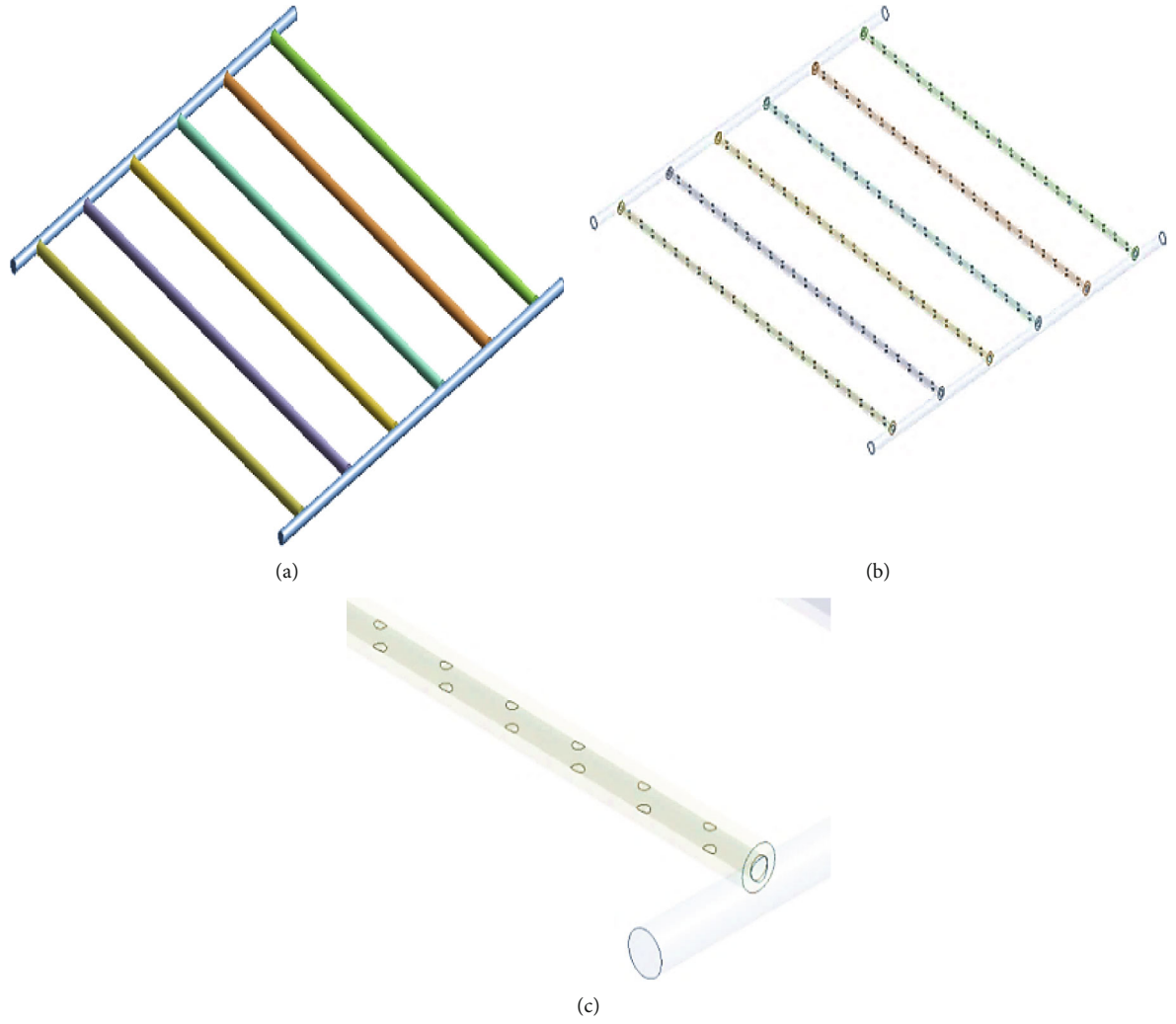

Figure 3: (a) Plain tube. (b) Dimpled tube. (c) Dimpled tube with nanofluid.

collector efficiency is shown in Equation (11). These values were compared to prior versions using the new one. The $F_R(\eta_c)$ and $\alpha\tau(F_R)$ intercept component with a linear regression approach. The collector's overall efficiency for SiO_2 at 0.3% has been 62.25% increased from 54.25% on the level of base fluid at a comparable flow rate based on the regression equation of the DI water and quality of the SiO_2 nanofluids. Experimental studies suggest that the highest exit temperate of $T = 93.15$˚C has been recorded due to the higher period of interaction between the recipient surface and the working fluid at a lower mass flow rate (0.5 kg/min–3.0 kg/min). In comparison, the temperature graduate of $\Delta T = (T_O - T_I)$ was lower at the peak flow rate ($m = 1.0$ kg/s) and corresponded to a more significant convective heat transfer coefficient. In this investigation, parameters such as friction factor, uncertainty analysis, Reynolds number, solar

collector efficiency, Nusselt number, and convective heat transfer coefficient were determined in the solar PTSC system.

2.7. Uncertainty Analysis. For analysis and regression techniques, all experimental values are averaged in numerical and CFD analysis. The uncertainties of the variable effects resulting from derived variables (η_c, Re, Nu, and f) were discovered in the experimental calculation of independent variables (T, Q_g). The standard deviation has been manipulated by derived Equation (12) since each variable has been measured over a minimum of three intervals.

$$\ni_R = \sqrt{\left[\left(\frac{\ni_1 \partial S}{\partial X_1}\right) + \left(\frac{\ni_2 \partial S}{\partial X_2}\right) + \left(\frac{\ni_3 \partial S}{\partial X_3}\right) + \cdots\cdots\cdots \left(\frac{\ni_N \partial S}{\partial X_N}\right)\right]}. \tag{12}$$

Based on Equation (12) [9], the proportional error is calculated as follows:

$$E_R = \frac{\ni_R}{S}\%. \tag{13}$$

Solar PTSC performance depends explicitly on normal direct irradiance, fluid inlet temperature, mass flow rate, and outlet temperature (η_c, Re, Nu, f, T, and Q_g). The following equation gives us clarity regarding the performance of the solar collector, as shown in [9, 18]

$$\eta_c = f\left(T_O, T_I, T, Q_g\right), \tag{14}$$

$$\ni_{\eta_c} = \sqrt{\left[\left(\frac{\partial \eta_c}{\partial Q_g} \ni_{T_O}\right) + \left(\frac{\partial \eta_c}{\partial T_I} \ni_{T_I}\right) + \left(\frac{\partial \eta_c}{\partial T_O} \ni_{Q_g}\right) + \cdots\cdots\cdots \left(\frac{\partial \eta_c}{\partial T} \ni_T\right)\right]}. \tag{15}$$

In Equation (16), flow rate with velocity (m/s) can be expressed as [9]

$$\ni_V = \sqrt{\frac{\partial V}{\partial m} \ni_m}. \tag{16}$$

In Equation (17), Nusselt number (Nu) with Reynolds number can be expressed as [9]

$$\ni_{\mathrm{Nu}} = \sqrt{\frac{\partial \mathrm{Nu}}{\partial\, \mathrm{Re}} \ni_{\mathrm{Re}}}. \tag{17}$$

In Equation (18), Reynolds number (Re) with velocity can be expressed as [9]

$$\ni_{\mathrm{Re}} = \sqrt{\frac{\partial\, \mathrm{Re}}{\partial \ni_V} \ni_V}. \tag{18}$$

In Equation (19), friction factor (f) with pressure drop (ΔP) can be expressed as [9]

$$\ni_f = \sqrt{\frac{\partial f}{\partial \Delta P} \ni_{\Delta P}}. \tag{19}$$

The field under curves was eventually used to compare cases for the collector's overall efficiency index.

3. Results and Discussion

3.1. Flow of Velocity. For validating the experimental analysis with simulation, the developed CFD models' velocity magnitude was compared with the experimental values. Furthermore, there was a positive correlation between the experimental values for CFD analysis, as shown in Figure 4. The magnitude of velocity has been determined in a steady state and utilized to determine the numerical model's prediction efficiency. The magnitude velocity displays the effects of the velocity contour in the dimples tube. The flow behaviour is almost identical in both experimental and CFD analysis, as illustrated in Figure 4. Flow behaviour demonstrates a fair and accurate estimation process and numerical procedure. In the experimental analysis, nanoparticles of SiO_2 containing the volume of concentration 0.1-0.5 percent were used to absorb the SiO_2 levels in a solar dimpled tube. The base fluid, nanoparticles, and nanofluid thermophysical properties are comparatively analyzed.

3.2. Temperature Contour. The dimpled tube temperature contour at different inclination angles with different nanofluid levels for PTSC is shown in Figure 5. The dimpled tube flow is bailment-based, where the SiO_2 nanofluid fills the outer core of the dimpled tube, where the cold water from the tank is passed through the inner core of the dimpled tube. The inclination angle of the PTSC rises from 30° to 60°. At the same time, the dimpled tube temperature decreases because of a reduced buoyancy strength produced in the vicinity of a tube and tank joint. Furthermore, the greatest velocity and temperature have been achieved at a volume fraction of 0.3 percent in all angles. The magnitude plot of 0.1-0.5% nanofluid and three distinct inclination angles at the tube inlet are analyzed. Results showed that the dimpled tube flow velocity at a tilt angle of 45° was recorded to be high. SiO_2 fluid has been assumed to significantly influence thermosiphon phenomena at the analysis phase, contributing to the above results.

3.3. Pressure Contour. The disparity between average Nusselt numbers and volume spacing is shown in Figure 6 for the various inclination angles from 30° to 60°. The average Nusselt number increases for all inclination angle values with the increment in volume fraction. However, the rising inclination angle reduces the mean amount of Nusselt number for the entire volume fraction concentration. This is induced by developing and reducing the mean Nusselt number of the weak secular recirculation at the higher inclination angles. The adjustments in the Nusselt number in the heated walls for 0.5 percent volume at different angles are observed.

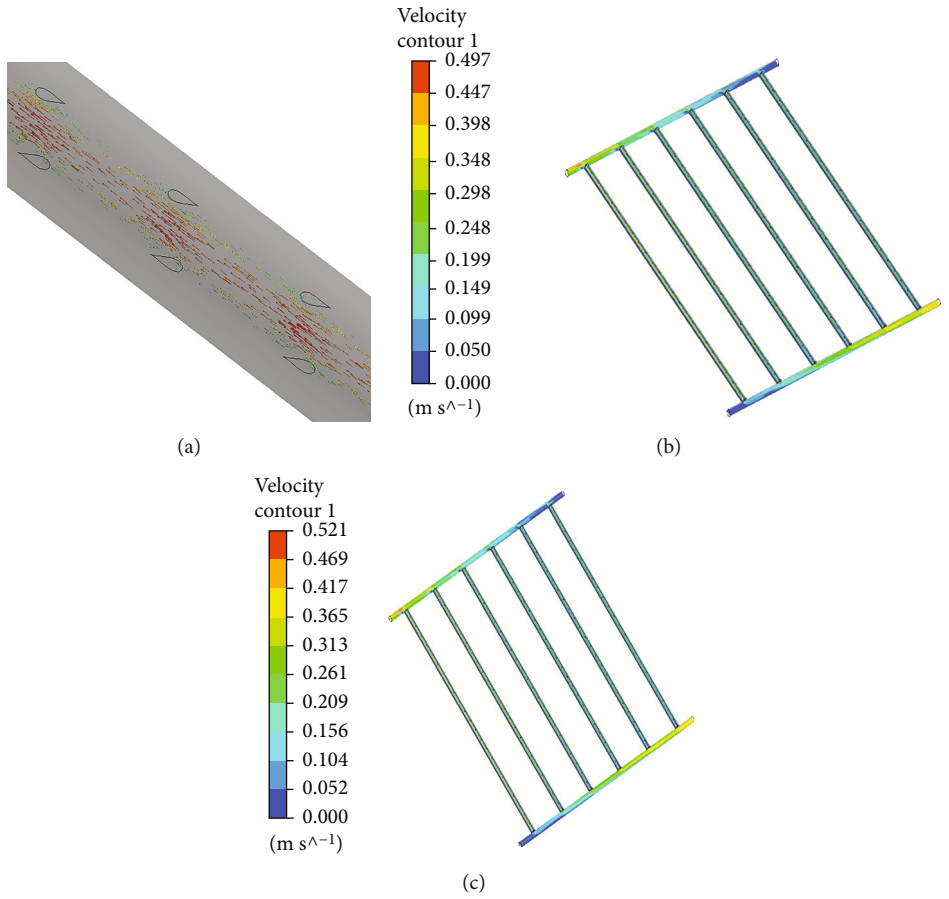

Figure 4: (a) Flow of water in dimpled tube. (b) Low velocity with low flow rate. (c) High velocity with high flow rate.

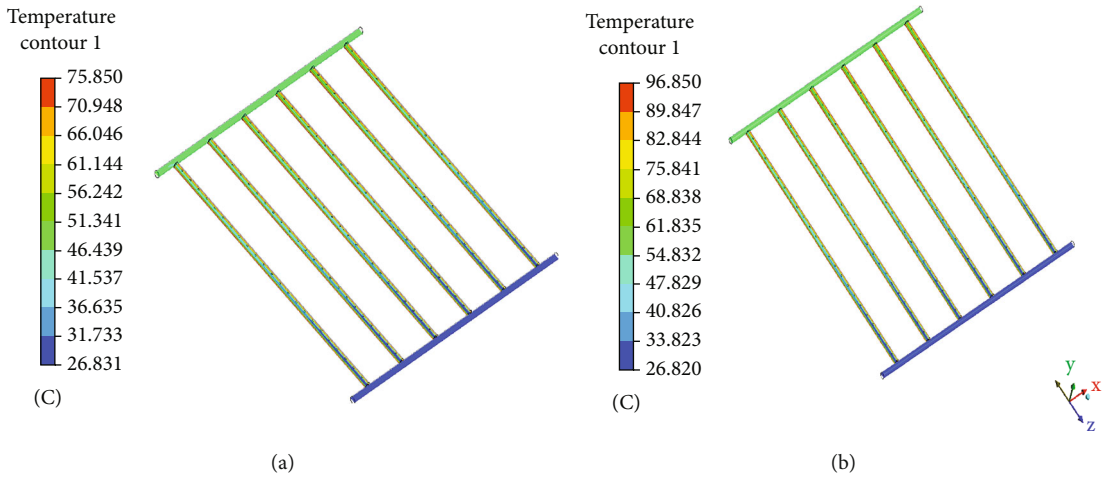

Figure 5: (a) Analysis of low temperature. (b) Analysis of high temperature.

The experimental outcomes confirmed that the higher Nusselt numbers are attained at a small inclination angle.

3.4. Comparison Absolute Energy. Figure 7 shows the energy consumed $\alpha\tau(F_R)$ with the variation in flow velocity for different concentrations of nanoparticles.

A maximum range of 5.43% greater than the base fluid has been observed in the 0.5 kg/min mass flow rate. The inclusion of SiO_2 nanoparticles is utilized to increase the absorbed energy factor, and it depends on the velocity of nanoflows, thermal conductivity, and basic heat power of the operating fluid. The heat absorption of nanoparticles is

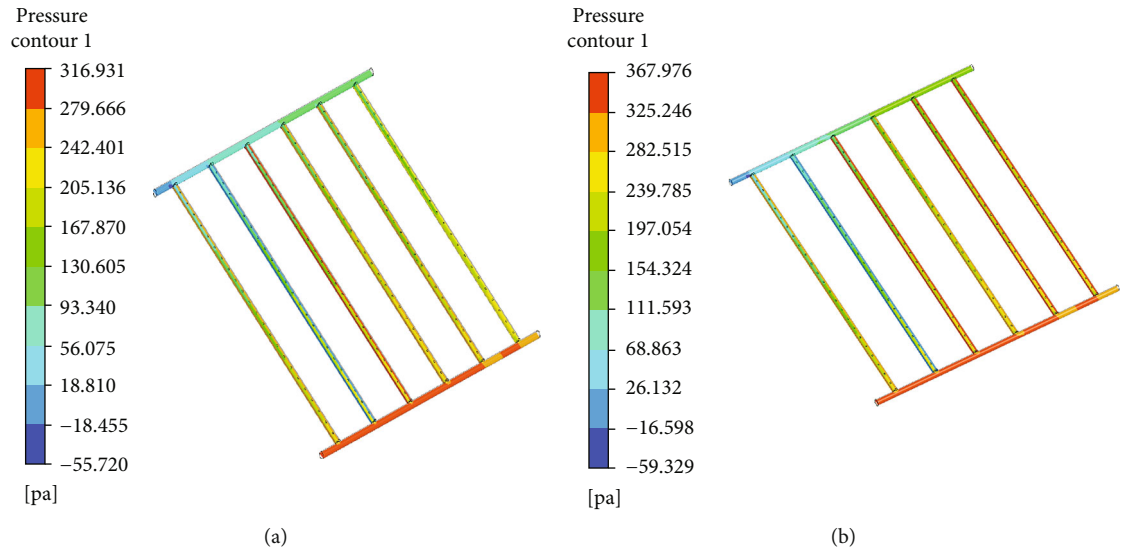

Figure 6: (a) Low-pressure contour. (b) High-pressure contour.

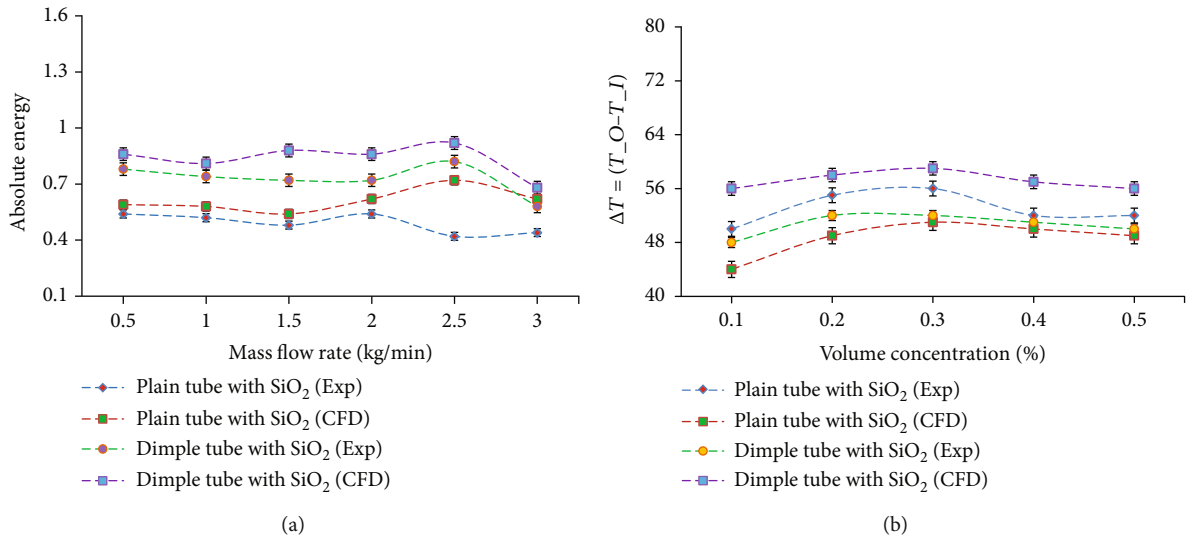

Figure 7: (a) Mass flow rates vs. absolute energy parameter. (b) Volume concentration vs. heat loss.

significantly improved at a volume concentration of 0.3% because the flow rate decreases and the fluid viscosity increases. Furthermore, Reynolds number also decreased. As a result, it contributed to the reduction in the thermal transfer coefficient and reduced the Nusselt number. The energy factor is absorbed for three different flow rates with the relative temperature of PTSC curves (0.5 kg/min-3.0 kg/min). For each of the flow rates, the efficiency is determined by the heat loss parameter $\Delta T = (T_O - T_I)$. The optimum collector efficiency of 62.35% was observed at flow rate of 2.5 kg/min and nanoparticle volume concentration of 0.3%. The variation in Nusselt number and Reynolds number is directly proportional to the heat augmentation rate. The working fluid in the dimpled tube with 0.3% of volume concentration of nanoparticles, at 2.5 kg/min, increases the Nusselt number by 2.5 times compared to the plain tube. It clearly shows that the presence of dimples significantly affected the improvement in heat transfer rate.

3.5. Analysis of Collector Efficiency. Figure 8 shows the collector efficiency improved by 11% and that the convective heat transfer increased by 34.25% relative to the base fluid. The collector efficiency and heat transfer have been enhanced due to increased SiO_2 nanoparticles' absorbance and absorption coefficient. Consequently, a pressure drop in the gradient temperature increased the convective heat transfer coefficient for nanofluids as expressed as $\Delta T = (T_O - T_I)$. For higher volume concentrations (0.1 to 0.5%), there is an 11% improvement in the solar PTSC quality compared with base fluid. The finding shows that the collector efficiency

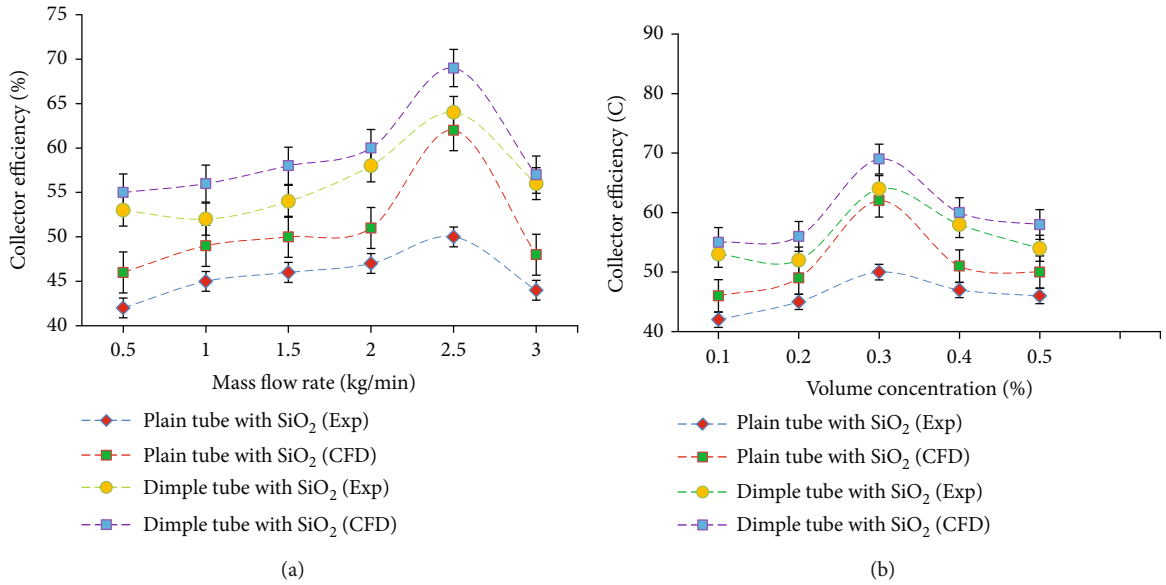

Figure 8: (a) Mass flow rate vs. collector efficiency (%). (b) Volume concentration vs. collector efficiency (%).

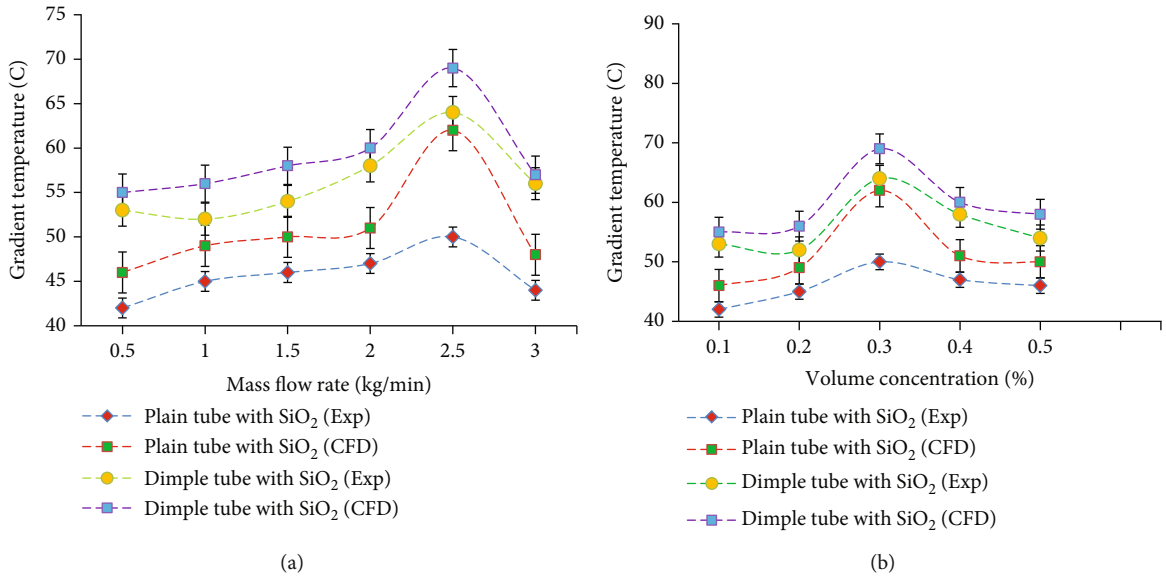

Figure 9: (a) Mass flow rate vs. gradient temperature. (b) Volume concentration vs. gradient temperature.

has been improved by 0.4%, while the volume concentration is rising by 0.5% at the various flow speeds. Since solar PTSC performance increased by an average of 0.5%, the volume's optimum concentration decreased to 0.3%. The flow rate is often shown to be inversely proportional to the temperature of the gradient. As a result, the flow rate increased, and the heat transfer coefficient improved in SiO_2 with the dimpled tube resulting in a significant improvement in the collector's performance.

3.6. Analysis of Gradient Temperature. Figure 9 depicts the temperature gradient maps at varying flow rates and concentrations of SiO_2 nanoparticles and convective heat transfer coefficients at different flow rates. These two graphs would conveniently correlate the temperature, flow rate difference, and heat transmission coefficient. Furthermore, the temperature difference is minimal, and the heat transfer coefficient is proportionally greater at velocity variance. The heat transfer coefficient is smaller during higher flow rates of the contact time on the surface (flow over time). At the same time, the heat transfer coefficient is higher at a lower flow rate. For nanofluids, a temperature gradient of 28.322°C has been achieved at a lower mass flow rate and a temperature gradient of 7.45°C at a higher velocity flow rate.

3.7. Effect of Nusselt Number. The velocity flow and concentration plots are illustrated in Figure 10 for experimental and expected Nusselt numbers. An error value of ±3.12% has

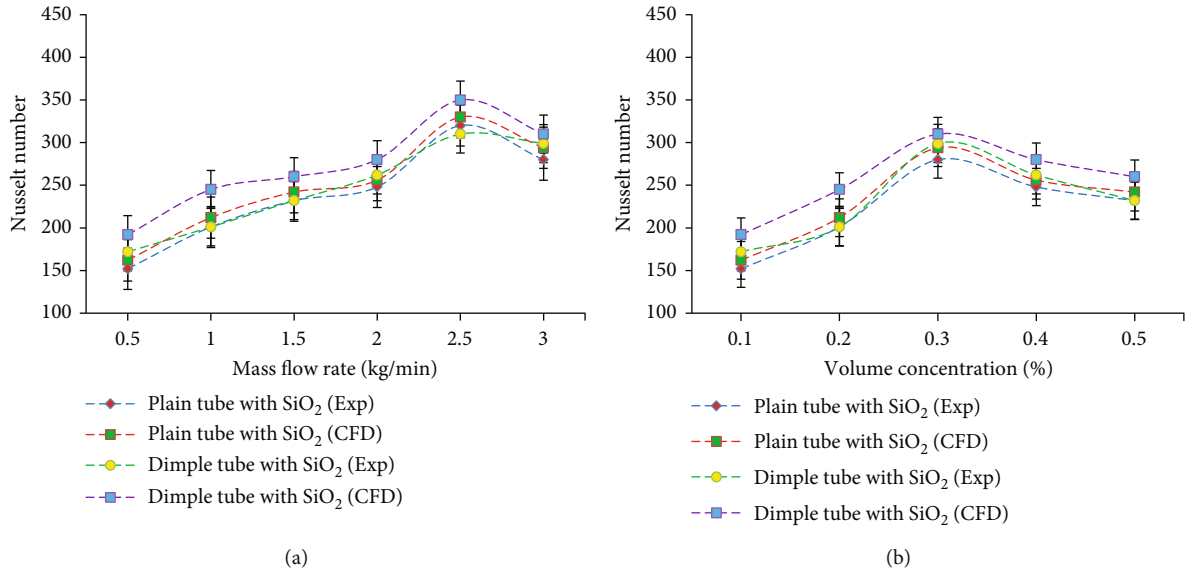

Figure 10: (a) Mass flow rate vs. Nusselt number. (b) Volume concentration vs. Nusselt number.

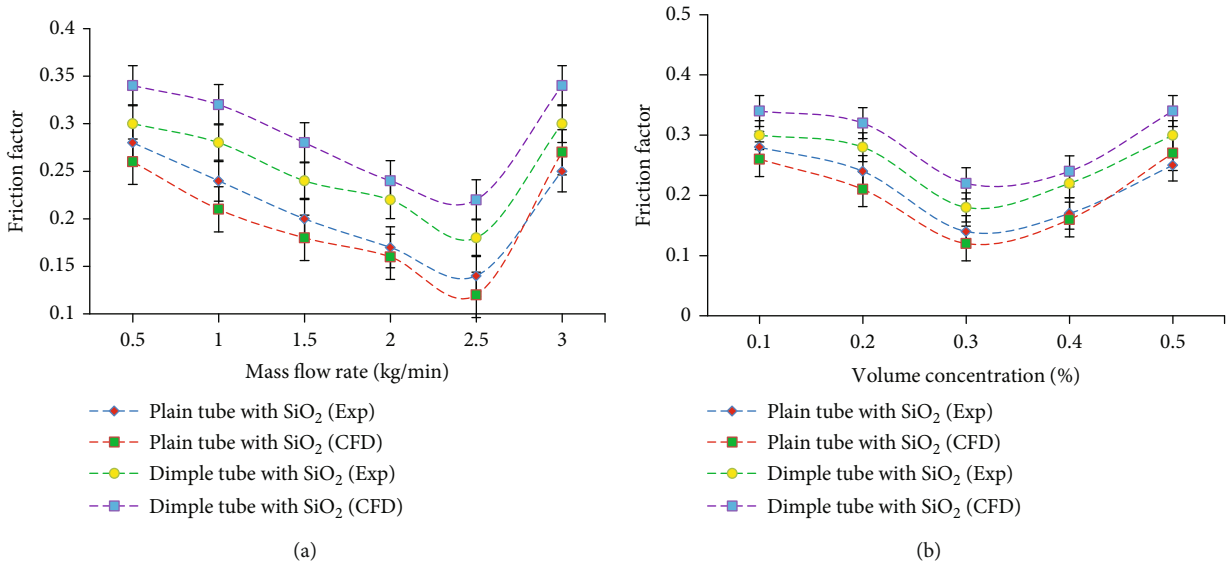

Figure 11: (a) Mass flow rate vs. friction factor. (b) Volume concentration vs. friction factor.

been observed between the CFD analysis and experimental values. Empirical correlation calculations are performed based on varying volume concentrations and velocity flow rates as per Equations (16) and (17) for different Reynolds numbers and Nusselt numbers. The developed model significantly improved the collector efficiency by 62.32% for the Reynolds number range of ($3256 < Re < 9685$) and Prandtl (6.324 to 9.254). Based on the outcomes obtained from CFD and experimental analysis, a volume concentration of 0.3% at 2.5 kg/min exhibits an 11% increment in heat transfer efficiency compared to other flow characteristics.

3.8. Effect of Friction Factor. The experimental and CFD analysis plots for friction factors with various concentrations and flow rates are illustrated in Figure 11. The friction factor is measured as a product of pressure drop and the surface roughness of the dimpled tube. Furthermore, the average pressure drop is recorded as 2.36 kPa for the solar PTSC system. In the current model, the deviation from the estimated friction factor is roughly ±4.62%. The expected friction factor for a higher Reynolds number can deviate in a range of ±11%. The efficiency metrics of experimental and CFD analysis with various flow rates and concentrations of nanoparticles and the deviations can be recorded as approximately ±7.42% percent. It shows efficiency index combinations for different Reynolds numbers and concentrations of nanoparticles. At 0.1-0.5% of the volume concentrations and a volume flow rate of 2.5 kg/min, the maximum output

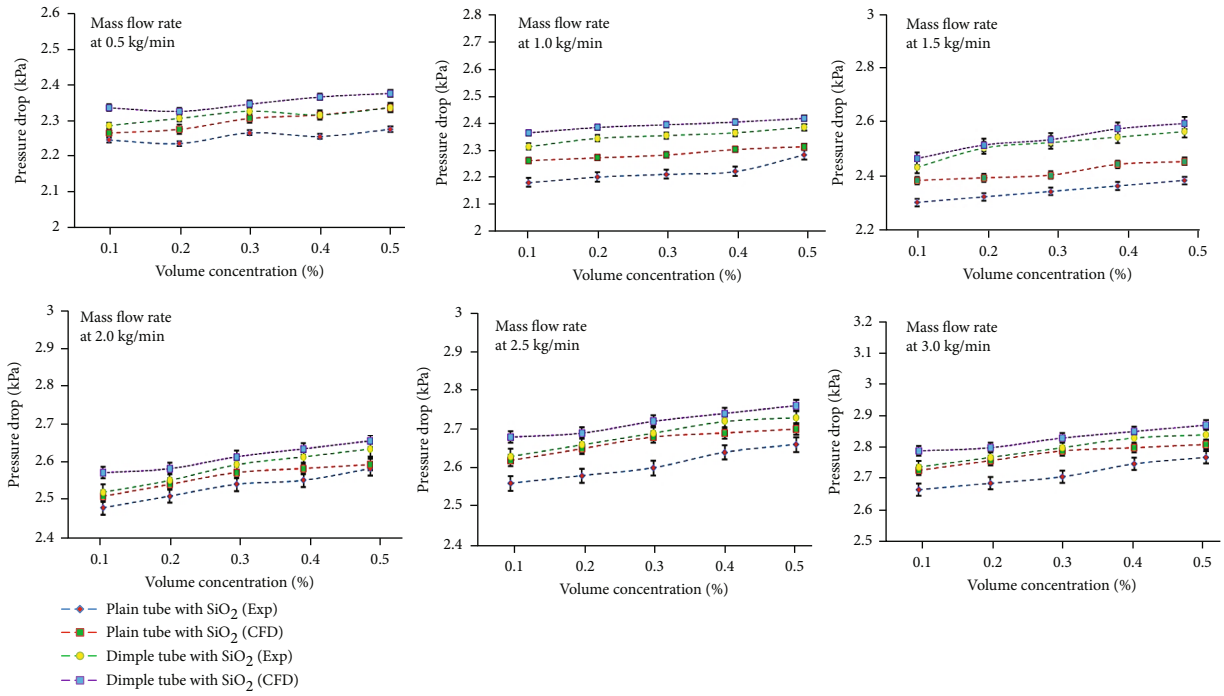

Figure 12: Variation of pressure drop with variation in nanoparticle volume concentration and mass flow rate.

index is 2.42. The SiO_2 nanofluid output index is larger than 1; in the PTSC application, the heat transfer increased in this research. The efficiency variations are based on pH changes and thermophysical nanofluid properties of SiO_2. Particle size affects the solar performances of PTSCs. Nanoparticles of more significant sizes tend to spread and absorb radiation. The measurement of the SiO_2 nanoparticles should be 50 nm to provide efficient heat transfer rates. In this analysis, the average size of the SiO_2 nanoparticles is 50 nm. The heat transfer has been improved in this research, and SiO_2 nanoparticles were efficient for PTSC solar applications.

3.9. Variation of Pressure Drop Concerning Dimpled Texture Tube. Figure 12 portrays the variation of pressure drop with the variation in nanoparticle volume concentration and mass flow rate. From Figure 12, it is observed that with an increase in the concentration of nanoparticles, the pressure drop increases irrespective of the mass flow rate of the water. This is due to the rise in the volume density of the nanoparticles in the nanofluid, which resulted in a more viscous flow of the nanofluid due to an increase in density. From Figure 12, it was also observed that dimpled tubes with SiO_2 nanoparticles exhibited a higher drop in pressure compared to the plain tube with SiO_2. This is due to increased obstacles to fluid flow due to dimple texturing on the tube surface. Apart from this, the dimpled texture offers more drag force to be experienced by the molecules adjacent to the inner tube layer during its dynamic condition. The pressure drop of the solar water heater has increased gradually with the increase in the mass flow rate of water. At a maximum mass flow rate of 3.0 kg/min and 0.5% volume concentration, the pressure drop has been increased by around 5.5% compared to the mass flow rate of 2.5 kg/min. The errors observed in the experiment and simulation are 6.2% and 2.5%, respectively, indicating the linear relationship between the experiment and simulation outcomes. Furthermore, the pressure drop results of the experimental condition are significantly higher than the simulation results.

4. Conclusions

The research analyzed SiO_2 efficiency in heat transfer for solar PTSC applications. Tests were performed using various concentrations of nanoparticles and mass flow rates. The numerical prediction was made on the SiO_2/water nanofluid collector, evacuated by thermosiphon, using commercial ANSYS tools. For various conduit angles, the effect of nanoparticle volume fraction on the collector's thermal efficiency was studied. The most significant conclusions achieved in this study are as follows:

(1) The nanoparticle volume fraction increases the heat conductivity and Nusselt number of solar evacuation pipes

(2) The inclination of 45° plays a significant role in enhancing the thermal efficiency and increases the evacuated tunnel's thermosiphon effect

(3) At the nanoparticle volume fraction and angle of inclination of 0.3 percent and 45 degrees, respectively, the optimum speed and heat transfer change were observed

(4) The nanofluid's output index is 2.42 with a 0.3% mass flow rate and concentration of 2.5 kg/s. The PSPC with SiO_2 nanofluid has a maximum overall

efficiency of 34.25%, which is 11% higher than that of the base fluid

Adopting this technology in operating the solar water heater may enhance heat transfer efficiency. This technology will provide added advantages to commercial solar water heaters in both the industrial and domestic sectors.

Data Availability

The data are available within this manuscript.

Conflicts of Interest

The authors declare that they have no conflict of interest.

Acknowledgments

The authors sincerely thank the Karpagam Academy of Higher Education (KAHE), Coimbatore, India, and Kampala International University, Western Campus, Kampala, Uganda, for providing the necessary facilities to carry out the research.

References

[1] S. T. Hamidi, "A novel application for parabolic trough solar collector based on helical receiver tube and nanofluid with a solar tracking mechanism," *Engineering and Technology Journal*, vol. 38, no. 5, pp. 656–668, 2020.

[2] A. Y. Al-Rabeeah, I. Seres, and I. Farkas, "Thermal improvement in parabolic trough solar collector using receiver tube design and nanofluid," *In International Workshop IFToMM for Sustainable Development Goals*, vol. 108, pp. 30–40, 2021.

[3] A. K. Tiwar, V. Kumar, Z. Said, and H. K. Paliwal, "A review on the application of hybrid nanofluids for parabolic trough collector: Recent progress and outlook," *Journal of Cleaner Production*, vol. 292, article 126031, 2021.

[4] R. Naveenkumar, M. Ravichandran, B. Stalin et al., "Comprehensive review on various parameters that influence the performance of parabolic trough collector," *Environmental Science and Pollution Research*, vol. 28, no. 18, pp. 22310–22333, 2021.

[5] J. Subramani, P. K. Nagarajan, O. Mahian, and R. Sathyamurthy, "Efficiency and heat transfer improvements in a parabolic trough solar collector using TiO_2 nanofluids under turbulent flow regime," *Renewable Energy*, vol. 119, pp. 19–31, 2018.

[6] M. Rezaeian, M. S. Dehaj, M. Z. Mohiabadi, M. Salarmofrad, and S. Shamsi, "Experimental investigation into a parabolic solar collector with direct flow evacuated tube," *Applied Thermal Engineering*, vol. 189, article 116608, 2021.

[7] S. E. Ghasemi, S. Mohsenian, and A. A. Ranjbar, "Numerical analysis on heat transfer of parabolic solar collector operating with nanofluid using Eulerian two-phase approach," *Numerical Heat Transfer, Part A: Applications*, vol. 80, no. 9, pp. 475–484, 2021.

[8] T. Sajid, W. Jamshed, F. Shahzad et al., "Study on heat transfer aspects of solar aircraft wings for the case of Reiner-Philippoff hybrid nanofluid past a parabolic trough: Keller box method," *Physica Scripta*, vol. 96, no. 9, p. 095220, 2021.

[9] M. Arun, D. Barik, K. Sridhar, and G. Vignesh, "Performance analysis of solar water heater using Al_2O_3 nanoparticle with plain-dimple tube design," *Experimental Techniques*, pp. 1–14, 2022.

[10] T. Sajid, W. Jamshed, F. Shahzad, M. R. Eid, E. K. Akgül, and K. S. Nisar, "Entropy analysis and thermal characteristics of Reiner Philippoff hybrid nanofluidic flow via a parabolic trough of solar aircraft wings: Keller box method," vol. 96, p. 9, 2021.

[11] W. Bai, Z. Zhang, W. Tian et al., "Toxicity of zinc oxide nanoparticles to zebrafish embryo: a physicochemical study of toxicity mechanism," *Journal of Nanoparticle Research*, vol. 12, no. 5, pp. 1645–1654, 2010.

[12] M. Moravej, M. V. Bozorg, Y. Guan et al., "Enhancing the efficiency of a symmetric flat-plate solar collector via the use of rutile TiO_2-water nanofluids," *Sustainable Energy Technologies and Assessments*, vol. 40, article 100783, 2020.

[13] O. Mahian, L. Kolsi, M. Amani et al., "Recent advances in modeling and simulation of nanofluid flows-part I: fundamentals and theory," *Physics Reports*, vol. 790, pp. 1–48, 2019.

[14] S. Parvin, R. Nasrin, and M. A. Alim, "Heat transfer and entropy generation through nanofluid filled direct absorption solar collector," *International Journal of Heat and Mass Transfer*, vol. 71, pp. 386–395, 2014.

[15] A. R. Noghrehabadi, E. Hajidavalloo, and M. Moravej, "An experimental investigation on the performance of a symmetric conical solar collector using SiO_2/water nanofluid," *Transp Phenom Nano Micro Scales*, vol. 5, pp. 23–29, 2016.

[16] M. Ghalambaz, A. Behseresht, J. Behseresht, and A. Chamkha, "Effects of nanoparticles diameter and concentration on natural convection of the Al_2O_3-water nanofluids considering variable thermal conductivity around a vertical cone in porous media," *Advanced Powder Technology*, vol. 26, no. 1, pp. 224–235, 2015.

[17] S. V. Sujith, A. K. Solanki, and R. S. Mulik, "Experimental evaluation in thermal conductivity enhancement and heat transfer optimization of eco-friendly Al_2O_3–pure coconut oil based nano fluids," *Journal of Thermal Science and Engineering Applications*, vol. 13, no. 3, article 031005, 2021.

[18] S. K. Verma, A. K. Tiwari, and D. S. Chauhan, "Experimental evaluation of flat plate solar collector using nanofluids," *Energy Conversion and Management*, vol. 134, pp. 103–115, 2017.

[19] S. Yan, F. Wang, Z. Shi, and R. Tian, "Heat transfer property of SiO_2/water nanofluid flow inside solar collector vacuum tubes," *Applied Thermal Engineering*, vol. 118, pp. 385–391, 2017.

[20] T. Yousefi, F. Veysi, E. Shojaeizadeh, and S. Zinadini, "An experimental investigation on the effect of Al_2O_3-H_2O nanofluid on the efficiency of flat-plate solar collectors," *Renewable Energy*, vol. 39, no. 1, pp. 293–298, 2012.

[21] L. S. Sundar and K. V. Sharma, "Numerical analysis of heat transfer and friction factor in a circular tube with Al_2O_3 nanofluid," *International Journal of Dynamics of Fluids*, vol. 4, pp. 121–129, 2008.

[22] R. Ekiciler, "CFD analysis of laminar forced convective heat transfer for TiO_2/water nanofluid in a semicircular cross-sectioned micro-channel," *Journal of Thermal Engineering*, vol. 5, pp. 123–137, 2019.

[23] M. R. Thansekhar and C. Anbumeenakshi, "Experimental investigation of thermal performance of microchannel heat sink with nanofluids Al_2O_3/water and SiO_2/water," *Experimental Techniques*, vol. 41, no. 4, pp. 399–406, 2017.

[24] P. Kalidoss, S. Venkatachalapathy, and S. Suresh, "Optical and thermal properties of Therminol 55-TiO_2 nanofluids for solar energy storage," *International Journal of Photoenergy*, vol. 2020, Article ID 7085497, 9 pages, 2020.

[25] B. N. Cardoso, E. C. Kohlrausch, M. T. Laranjo et al., "Tuning anatase-rutile phase transition temperature: TiO_2/SiO_2 nanoparticles applied in dye-sensitized solar cells," *International Journal of Photoenergy*, vol. 2019, Article ID 7183978, 9 pages, 2019.

[26] A. Ayoobi and M. Ramezanizadeh, "An exhaustive review on a solar still coupled with a flat plate collector," *International Journal of Photoenergy*, vol. 2021, Article ID 9744219, 24 pages, 2021.

[27] Y. Cao, H. Ayed, T. Abdulrazzaq, T. Gul, A. Bariq, and B. Bouallegue, "Effect of the number of nozzles of swirl flow generator utilized in flat plate solar collector: an entropic analysis," *International Journal of Photoenergy*, vol. 2021, Article ID 8320714, 10 pages, 2021.